Monte Carlo simulation of electron scattering and secondary electron emission in individual multiwalled carbon nanotubes: A discrete-energy-loss approach

M. K. Alam and A. Nojeh[a)]
Department of Electrical and Computer Engineering, The University of British Columbia, 2332 Main Mall, Vancouver BC, V6T 1Z4, Canada

(Received 1 March 2011; accepted 2 June 2011; published 29 June 2011)

Electron scattering in and secondary electron emission from multiwalled carbon nanotubes are investigated using Monte Carlo simulation. The method treats energy loss in a discrete manner, resulting from individual scattering events, rather than within a continuous-slowing-down approximation. Simulation results agree fairly well with the reported experimental data. The effect of number of nanotube walls is investigated and the energy distribution of the transmitted electrons is calculated. It is found that secondary electron yield in the low-primary-energy range is more sensitive to the number of walls and is maximized for a particular number of walls. The effect is not significant in the higher-primary-energy range. The effect of core electron ionization on secondary electron emission from nanotubes is found to be negligible because of the low scattering cross-section involved. The presented framework can also be applied to other small structures such as nanowires. © *2011 American Vacuum Society.* [DOI: 10.1116/1.3605300]

I. INTRODUCTION

Carbon nanotubes (CNTs) have many interesting electrical, mechanical and optical properties. Previous studies have shown the potential of CNTs for nanoscale devices, as well as in vacuum electronic applications requiring stable, low-voltage electron emitters, electron multipliers, etc.[1–5] Yet, electron emission mechanisms in CNTs are not fully understood. It is not entirely clear how nanotubes interact with electron beams and emit secondary electrons (SEs), or why a CNT, despite its nanoscale diameter and hollow structure, is readily visible in a scanning electron microscope. SE emission plays a vital role in the imaging of CNTs using electron microscopy.[6–8] In addition to being of fundamental scientific interest, understanding the interaction between a primary electron beam and nanotubes is crucial in designing electron emission devices, imaging/characterizing nanotube-based devices and circuits or calculating their X-ray spectra. Monte Carlo simulation of the interaction of electron beams with individual CNTs can provide useful information (e.g., SE yield of CNTs/CNT-based devices) and insight in this context. Monte Carlo simulation has been the most common approach to modeling the interaction of electron beams with solids. In this method, each electron trajectory is created from a series of random scattering events.[9,10] This technique has been used to predict various phenomena such as electron backscattering and energy dissipation in solids with considerable success.[9–16] However, secondary electron emission has proven more difficult to deal with.[9,17] Conventional Monte Carlo simulators typically use Bethe's energy loss model (or a modified version of it) based on the continuous-slowing-down approximation (CSDA). Hence, they cannot be directly applied when the structure is smaller than the random step length and an incoming electron occasionally loses a large fraction of its energy in a single collision or in a few collisions. Examples of such structures are CNTs and nanowires. CNTs are hollow cylindrical structures made of carbon with diameters of a few nanometers to a few tens of nanometers. Therefore, a Monte Carlo model incorporating discrete energy loss events seems to be a more appropriate approach for CNTs.

Hybrid Monte Carlo models have also been proposed in order to include more details of the various phenomena in the simulation.[18] An early effort was made by Shimizu *et al.* who introduced discrete energy loss events in Monte Carlo simulation of bulk materials.[13,19] To the best of our knowledge, no model has yet been reported for simulating electron trajectories in individual CNTs. Recently, we reported experimental SE yield data for multiwalled carbon nanotubes (MWNTs).[20] Here, we perform a direct Monte Carlo simulation for such MWNTs, calculating the electron energy loss as a result of discrete scattering events, and compare the results with experimental data. We also discuss the energy distribution of the transmitted electrons and the effect of the number of CNT walls on SE emission.

II. MODELING

We defined a MWNT using its inner diameter and number of walls. The outer diameter was calculated based on the inner diameter and number of walls using an inter-wall distance of 0.34 nm.[21] Electron trajectories in individual CNTs (presented in the results and discussion section) were calculated using a discrete-energy-loss approach, discussed below. We used MWNTs with an inner diameter of 10 nm in this work, which is typical of the CNTs used in our previous experiments.[22,23] Our approach is based on the one proposed by Shimizu *et al.*[13,19] We used a different cross-section to

a)Electronic mail: anojeh@ece.ubc.ca

define the elastic scattering events.[12] For inelastic scattering, we considered the following three most significant mechanisms: Outer-shell electron ionization, core-shell electron ionization and plasmon excitation. In addition, we added the SE emission simulation capability.

Several experimental and theoretical works have been reported on the electron energy loss spectra of nanotubes, revealing the fundamental excitation processes in them.[24,25] In addition to the most common and prominent loss mechanisms (considered here), some very-low-energy loss peaks close to the elastic peak have been observed. For example, peaks at 90 meV and 170 meV for single-walled CNTs have been recorded by reflection energy loss spectroscopy.[25] These side peaks have been attributed to the excitation of various phonons.[25,26] Thus, a primary electron can lose only a few tens of meV in such processes, which is negligible compared to its kinetic energy (~0.5 to 30 keV for scanning electron microscopy). Therefore, the energy loss due to phonons can be neglected and electron-nucleus interaction was considered as entirely elastic here, similar to the case of bulk solids in typical Monte Carlo simulations of electron trajectories.

A brief description of the different cross-sections, the energy loss and secondary emission model, and the Monte Carlo procedure is given in the next sub-sections.

A. Scattering cross-sections and mean free paths

The empirical total cross-section proposed by Browning *et al.* was used for calculating the elastic mean free path (MFP) as[9,12]

$$\lambda_{el} = \frac{A}{\rho N_A \sigma_{el}}, \tag{1}$$

where A is the atomic weight, N_A is the Avogadro number, ρ is the density of the material and

$$\sigma_{el} = \frac{3 \times 10^{-18} Z^{1.7}}{E + 0.005 Z^{1.7} E^{0.5} + 0.0007 Z^2 / E^{0.5}} \tag{2}$$

is the total elastic cross-section in cm^2, where Z is the atomic number and E is the electron energy in keV.

The Møller scattering formula in the non-relativistic form was used for calculating the differential inelastic cross-section for outer-shell ionization as[18,27]

$$\frac{d\sigma}{dW} = \frac{\pi e^4}{(4\pi\varepsilon_0)^2 E}\left(\frac{1}{W^2} + \frac{1}{(E-W)^2} - \frac{1}{W(E-W)}\right), \tag{3}$$

where E is the initial energy of the incident electron, W is the energy loss suffered by it, e is the charge of the electron and ε_0 is the permittivity of vacuum.

The Gryzinski differential cross-section was used for the core-shell ionization process. It incorporates the binding energy of the shell and has proven successful for several solids.[18,19,28] It is calculated as[27]

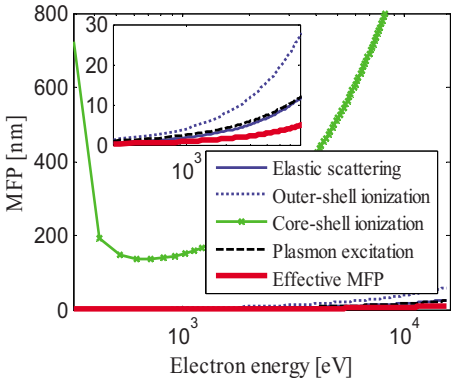

FIG. 1. (Color online) MFPs for the different scattering processes and the effective MFP as a function of electron energy. Inset shows the zoomed-in view (the core-shell scattering MFP is out of the scaled range).

$$\frac{d\sigma}{dW} = \frac{\pi e^4}{(4\pi\varepsilon_0)^2}\frac{E_b}{EW^3}\left(\frac{E}{E+E_b}\right)^{\frac{3}{2}}\left(1-\frac{W}{E}\right)^{\frac{E_b}{E_b+W}}\left\{\frac{W}{E_b}\left(1 - \frac{E_b}{E}\right) + \frac{4}{3}\ln\left[2.7 + \left(\frac{E-W}{E_b}\right)^{\frac{1}{2}}\right]\right\}, \tag{4}$$

where all the variables are the same as in Eq. (3) and the additional variable E_b is the binding energy of the shell.

The total scattering cross-sections per electron for Møller and Gryzinski scattering were found by integrating Eqs. (3) and (4) with respect to W. The binding energy of the inner shell was taken to be 284.2 eV.[29] The MFP for these scattering events can be found from

$$\lambda_{M/G} = \frac{A}{\rho N_A Z_\gamma \sigma_{M/G}}, \tag{5}$$

where $\sigma_{M/G}$ is the total cross-section (M for Møller and G for Gryzinski) and Z_γ is the number of electrons in the corresponding shell (for carbon, 4 in the outer shell and 2 in the inner shell).

The MFP for plasmon creation has been derived theoretically as[30,31]

$$\lambda_p = 2a_B \frac{E}{\hbar\omega_p}\left(\ln\frac{(1+y_p)^{1/2}-1}{x-(x^2-y_p)^{1/2}}\right)^{-1}, \tag{6}$$

where $x = \sqrt{E/E_F}$, $y_p = \hbar\omega_p/E_F$, a_B is the Bohr radius, $\hbar\omega_p$ is the plasmon energy, and E_F is the Fermi energy.

The plasmon energy was taken to be 20 eV for CNTs. Experimentally, it has been reported that the plasmon peak occurs between 15 eV and 26.9 eV, irrespectively of the diameter and type of the CNT.[24]

The effective MFP was calculated from:

$$\frac{1}{\lambda_T} = \frac{1}{\lambda_{el}} + \frac{1}{\lambda_M} + \frac{1}{\lambda_G} + \frac{1}{\lambda_p}. \tag{7}$$

Figure 1 shows the different MFPs calculated from the above expressions and the effective MFP as a function of electron energy.

B. Energy loss

Unlike in the CSDA energy loss calculation, in our model the energy loss was calculated for discrete scattering events according to the following rules:

1. No energy is lost during an electron-nuclei (elastic) scattering process.
2. A fixed amount of energy, $\hbar\omega_p$, is lost during a plasmon excitation process.
3. For core-shell and outer-shell ionization, the random nature of the energy loss is implemented using the probability integral transform theorem,[19,28]

$$\int_{W_c}^{W} \frac{d\sigma}{dW} dW = R \int_{W_c}^{W_{\max}} \frac{d\sigma}{dW} dW, \tag{8}$$

where W_c is the cut-off energy (taken as 10 eV for Møller scattering and equal to the binding energy for Gryzinski scattering), $W_{\max}$ (the maximum amount of energy that can be lost for a particular process) is equal to $E/2$ for Møller and to E for Gryzinski scattering,[28] and R is a uniform random number between 0 and 1.

Before proceeding to use the described scattering cross-sections and MFPs for nanotubes, it is instructive to estimate how they perform in a bulk material (for example, graphite) compared to Bethe's modified CSDA formula,[32]

$$\left|\frac{dE}{ds}\right|_{\text{CSDA}} = 785\frac{\rho Z}{AE}\ln\left(\frac{1.166(E+tJ)}{J}\right)\text{eV/Å}, \tag{9}$$

where J is the mean ionization potential, t is an empirical factor (0.77 for carbon) and the other variables are the same as defined before (J and E are in eV).

We can calculate an equivalent average energy loss arising from the discrete events using the following:[27]

$$\left|\frac{dE}{ds}\right|_{\text{M/G}} = N_A\rho\frac{Z}{A}\int_{W_{\min}}^{W_{\max}} \frac{d\sigma}{dW} W dW, \tag{10}$$

$$\left|\frac{dE}{ds}\right|_{\text{P}} = \frac{\hbar\omega_p}{\lambda_p}, \tag{11}$$

where plasmon energy is taken to be 26 eV for graphite.[33]

As can be seen on Fig. 2, for the chosen parameters the sum $|dE/ds|_{\text{M}}+|dE/ds|_{\text{G}}+|dE/ds|_{P}$ closely follows dE/ds (CSDA), which indicates that the discrete energy loss scheme with these cross-sections may also be used for bulk materials.

C. Scattering angle distributions

The scattering angle of the incident electron for each individual scattering process was calculated as follows. The elastic scattering angle was estimated from a fitted Mott differential cross-section, which is composed of two parts:[12]

$$\cos\theta = 1 - \frac{2\alpha R}{1+\alpha-R} \text{ (Rutherford scattering)}, \tag{12}$$

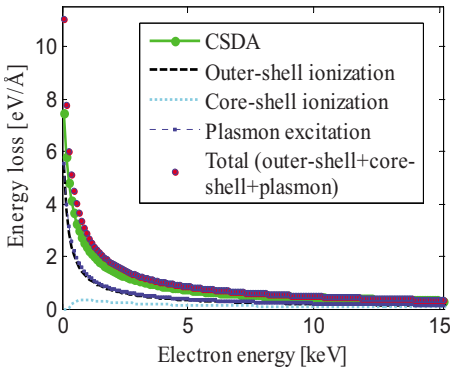

FIG. 2. (Color online) Comparison of the equivalent energy loss rate calculated from discrete processes with the CSDA energy loss.

$$\cos\theta = 1 - 2R \text{ (Isotropic scattering)}, \tag{13}$$

where α is the screening parameter and is calculated from

$$\alpha = \frac{7\times10^{-3}}{E}, \tag{14}$$

where E is in keV. The Møller scattering angle of the primary electron was calculated from[9,28]

$$\sin^2\theta_M = \frac{2E_n}{2+\mu-\mu E_n}, \tag{15}$$

where μ is the kinetic energy of the electron in the units of its rest mass (511 keV) and E_n equals W/E. The Gryzinski and plasmon scattering angles were calculated from[28,30,34]

$$\sin^2(\theta_{G/P}) = \frac{W}{E}. \tag{16}$$

Note that the elastic cross-section for very-low-energy scatterings does not have an analytical form and the cross-section proposed by Browning *et al.*[12] is reported for >100 eV. Nonetheless, in one approach we used Eqs. (12) and (13) due to their simple analytical form. Therefore, a correction was needed for the small portion of the elastic scattering processes happening below 100 eV. An alternative solution may be to use the tabulated data for the Mott cross-section.[35] Thus, we also used the interpolated values (from the Mott numerical data given down to 20 eV[36]) of elastic scattering angles and MFPs for higher accuracy in the lower energy range. Although the scattering cross-section by Browning *et al.*[12] is reported to be valid above 100 eV, we used the Mott cross-section up to 1 keV for better accuracy. Here, we present the results for both cases (with or without these corrections). We also note that there is some ambiguity present in the plasmon MFP below 80 eV where the logarithmic term becomes negative [see Eq. (6)]. The effect of this ambiguity reflects on the probability of plasmon scattering at lower energies and thus on the energy loss of the slow electrons. One simple solution might be to use extrapolated values down to the plasmon energy. All of these limitations just remind one of the fact that scattering at low energies is not yet completely understood and further fundamental study is needed. It may be possible to improve the cross-sections us-

ing empirical parameters. However, more fundamental experimental work is also needed in order to incorporate such corrections in a physically meaningful manner.

D. Monte Carlo procedure

The step length was calculated from:

$$s = -\lambda_T \ln R. \tag{17}$$

At each step of the simulation, the primary electron was scattered to a distance s away. The energy loss was calculated according to the description provided in section II.B and the entire loss was assumed to happen at the point of interaction. The scattering angles were estimated from Eqs. (12)–(16).

To find the energy loss and the scattering angle we also needed to determine the type of scattering at each step. It is known that the scattering probability is proportional to the inverse MFP. As the MFPs are known from Eqs. (5)–(7), we defined the probability of occurrence of each scattering process based on a uniform random number, R_s, as follows:

$$\begin{bmatrix} \text{elastic scattering: } 0 < R_s \le \dfrac{1/\lambda_{el}}{1/\lambda_T} \\ \text{plasmon excitation: } \dfrac{1/\lambda_{el}}{1/\lambda_T} < R_s \le \dfrac{1/\lambda_{el} + 1/\lambda_p}{1/\lambda_T} \\ \text{outer-shell ionization: } \dfrac{1/\lambda_{el} + 1/\lambda_p}{1/\lambda_T} < R_s \le \dfrac{1/\lambda_{el} + 1/\lambda_p + 1/\lambda_M}{1/\lambda_T} \\ \text{core-shell ionization: } \dfrac{1/\lambda_{el} + 1/\lambda_p + 1/\lambda_M}{1/\lambda_T} < R_s \le \left(\dfrac{1/\lambda_{el} + 1/\lambda_p + 1/\lambda_M + 1/\lambda_G}{1/\lambda_T} = 1 \right) \end{bmatrix}. \tag{18}$$

Based on the above inequalities, the type of scattering was determined and the corresponding set of equations was used for calculating the energy loss and the scattering angle.

Figure 3 shows the probability limits of different scattering processes for different primary beam energies [according to Eq. (18)]: A significant number of the primary electrons are elastically scattered without losing any energy. Very few of them excite the electrons in the core shell. Elastic scattering and plasmon excitation have comparable probabilities.

E. Secondary electron emission model for MWNTs

For CNTs, the role of each scattering process in generating SEs is still not clear. The most common mechanism of generating SEs seems to be valence electron ionization. In this work, we considered both outer-shell and core-shell ionization processes (the contribution from the core shell is very small as can be seen from Fig. 3). Also, there is no report in the literature on SE generation from plasmon decay in individual CNTs. Therefore, we neglected the SE generation probability from plasmon decay, that is we assumed that the primary electron energy loss causes the plasmon oscillation only, without exciting any single electron to a high enough energy to overcome the vacuum energy barrier.

It is also important to consider whether phonons can play a role in SE emission. Although phonons have low energy as discussed before, in principle it is possible for multiple phonons to transfer energy to one nanotube electron, assisting it in the emission process. Indeed, phonon-assisted electron emission has been reported for single-walled CNTs biased between two electrodes.[37] However, such a phenomenon has not been reported for SE emission from CNTs. Typically, it is also neglected in bulk solids for the considered energy range. Moreover, since the MFP for electron-phonon collision (on the order of micrometers for acoustic phonons and tens of nanometers for optical phonons[38]) is much larger than the CNT diameter, the chance of multiple phonon generation as the primary electron crosses the nanotube is very low, suggesting negligible probability of non-equilibrium phonon build-up and subsequent contribution to SE emission. For example, if a given CNT electron gains 90 meV of kinetic energy from phonon absorption, at least 50 phonon absorption events are needed to accumulate a kinetic energy equal to the minimum ionization

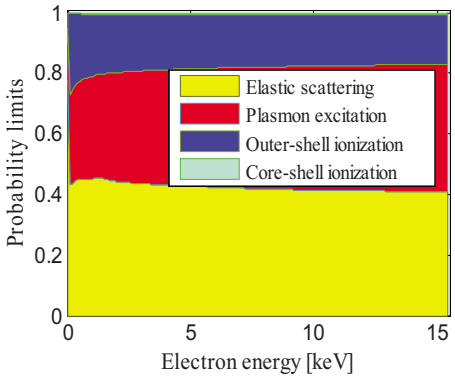

FIG. 3. (Color online) Probability of different scattering processes at different primary beam energies.

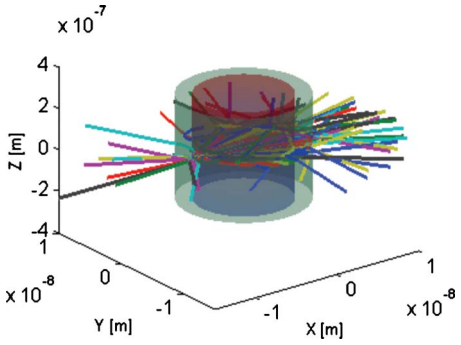

FIG. 4. (Color online) Electron trajectories in a MWNT for a 0.5-keV beam perpendicular to the CNT (No. of walls=6). Only 70 trajectories are plotted for clarity.

energy of nanotubes (~4.5 eV) to overcome the vacuum barrier. Therefore, electron-phonon interaction was not considered in the present work. Nevertheless, this phenomenon, if proven important in future, can be incorporated into the proposed simulation framework easily if the excitation cross-sections for phonon generation and absorption are theoretically known.

For each SE, the initial energy was assumed to be equal to the energy lost by the primary electron minus the corresponding binding energy (for core-shell or outer-shell). The initial scattering angle (θ_{SE}) for electrons generated by outer-shell ionization can be estimated from[9,28]

$$\sin^2 \theta_{SE,M} = \frac{2(1-E_n)}{2+\mu E_n}, \tag{19}$$

where μ is the kinetic energy of the electron in the units of its rest mass (511 keV) and E_n is equal to W/E. For core-shell ionization:

$$\cos^2(\theta_{SE,G}) = \frac{W}{E}. \tag{20}$$

Once a new electron was generated as a result of a scattering process, it was tracked using the same Monte Carlo procedure. If an electron exited the CNT with an energy of less than 50 eV, it was counted as an SE. Otherwise, it was counted as a backscattered electron.

III. RESULTS AND DISCUSSION

Electron trajectories for primary energies of 0.5 and 5 keV are shown in Figs. 4 and 5, respectively, for an incident beam perpendicular to the tube axis or at an angle (for the 5-keV case). As can be seen from the figures, the perpendicular beam goes almost straight through for higher energies. However, the number of scattering events inside the CNT increases if the beam hits the CNT at an angle relative to the surface normal [Fig. 5(b)].

The SE yield calculated from the simulation along with the available experimental data[20] is presented in Fig. 6. 10,000 trajectories were simulated at each primary-beam energy. The effect of number of walls is negligible in the range of 5–9 walls because the MFP (i.e., the random step length)

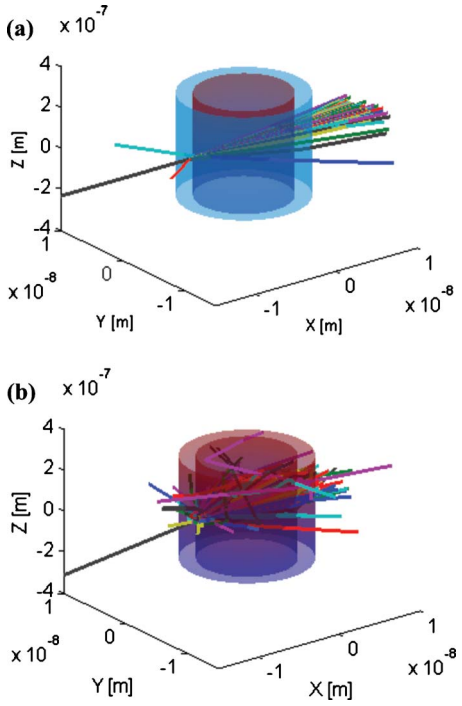

FIG. 5. (Color online) Electron trajectories in a MWNT for a 5-keV beam (No. of walls=6). Only 70 trajectories are plotted for clarity. (a) Beam perpendicular to the CNT axis and (b) beam oblique to the CNT (angles with the axes: $X=78°$, $Y=90°$ and $-Z=168°$).

is larger than the sidewall thickness for most of the energy range and, therefore, the number of scatterings does not depend on the number of walls. It was also seen that with the increase of the number of walls above 9 (not shown here), or its decrease below 5 walls, the SE coefficient decreases in the lower energy range. With a higher number of walls the probability of SEs escaping from the specimen decreases. On the other hand, the energy loss decreases for fewer walls because the number of scattering events decreases.

The effect of core-shell ionization on SE emission is shown in Fig. 7. The effect is negligible because the probability of core-shell ionization is very low (<1%) (see Fig. 3). The energy distribution of the transmitted electrons through the CNT (for 6 walls) is shown in Fig. 8 for two

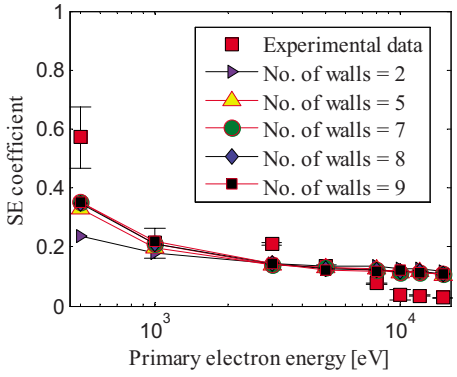

FIG. 6. (Color online) Simulated SE coefficient for different MWNTs, together with the experimental data reported in Ref. 20.

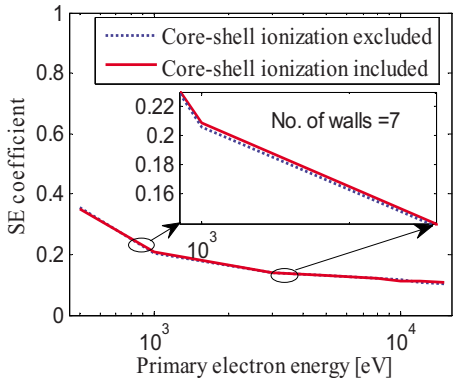

FIG. 7. (Color online) Simulated SE coefficients showing the effect of incorporating core-shell ionization.

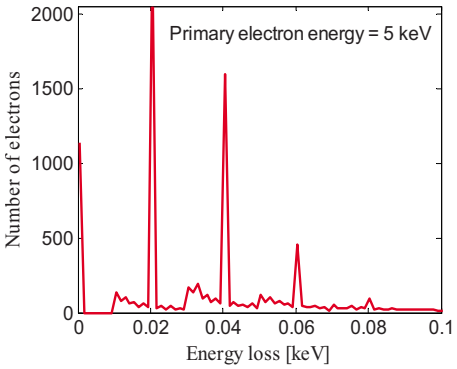

FIG. 9. (Color online) Energy loss distribution of the electrons (primary electron energy=5 keV).

different primary-beam energies. As expected, most of the primary electrons escape with minimal energy loss for higher beam energies. However, the transmitted electron energy has a wide distribution for lower incident beam energies [Fig. 8(a)].

Multiple peaks can be noticed on the energy loss distribution of a 6-wall CNT (Fig. 9): the zero-loss peak due to elastic scattering, the plasmon loss peak and a weak peak around the Møller cut-off energy. Similar peaks were theoretically calculated for and observed in electron-energy-loss-spectroscopy of CNTs.[24,39] It can also be noted that there are several strong peaks at integer multiples of the plasmon energy. The peaks arise because of the multiple scatterings of the primary electron (number of scatterings up to 5 in this case) in the CNT. As expected the relative strength of the peaks decreases with energy due to the lower probability of multiple scatterings. The energy loss due to outer-shell ionization extends to a wide energy range starting at the Møller cut-off energy.

Figure 10 shows that a better agreement with the experimental data in the higher energy range is achieved when the low energy corrections (discussed in section II.C) are incorporated. However, the difference with the experimental data is still maximal at 500 eV [underestimated by the simulation (Fig. 6)] and is further increased by ~35%. Plasmon excitation might play a very important role in this region and contribute to SE emission. Incorporating the contribution of plasmon excitation could potentially improve the low-energy fit. However, as mentioned earlier the contribution of plasmon excitation to the SE emission of CNTs is not well known. Also, inelastic scattering cross-sections for SE excitation from various materials are still not known very accurately. Nonetheless, the agreement is fairly good in the range of 1–15 keV, with a root-mean-square difference of 0.0406 between simulated and experimental results. Similar differences are also seen between simulated and experimental data for bulk materials,[17] and even between values reported in different experiments on the same material.[40] We thus be-

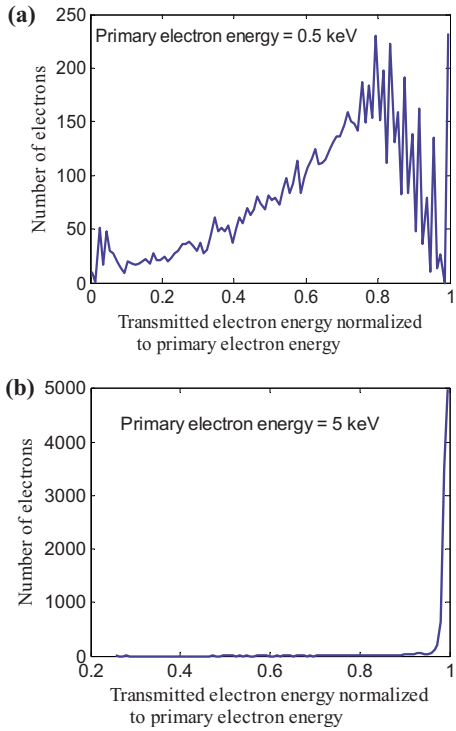

FIG. 8. (Color online) Energy distribution of the transmitted electrons. (a) primary electron energy=0.5 keV and (b) primary electron energy =5 keV.

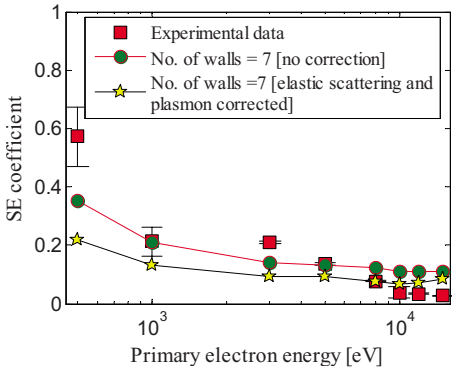

FIG. 10. (Color online) Simulated SE coefficients for a MWNT, with and without corrections for the lower energy plasmon and elastic scatterings, and comparison with the experimental data reported in Ref. 20.

lieve that the present work is a useful preliminary step toward the modeling of SE emission from nanotubes.

The framework presented here can also be used for nanotubes lying on a substrate, larger structures made of several nanotubes or other nanostructures such as nanowires (although for larger structures, such as CNT bundles, CSDA-based models could also be used[22,41]). We note that our simulation results suggest that SE yield is significantly lower at low primary beam energies for nanotubes with less than 5 walls (Fig. 6). Therefore, one would expect less SE emission from single-walled CNTs due to the outer-shell electron ionization. In addition, two plasmon modes have been reported for MWNTs compared to one for single-walled CNTs.[42] This suggests that the contribution of plasmon excitation and, therefore, the total SE yield of single-walled CNTs should be less than those of MWNTs, although other mechanisms could also play a role.[43] This also agrees with the experimental observation that MWNTs are typically more readily visible in scanning electron microscopy than single-walled CNTs.

IV. SUMMARY AND CONCLUSIONS

We used a discrete-energy-loss approach for the Monte Carlo simulation of SE emission from individual CNTs. Such a model, although previously proposed for bulk materials, may not have been in widespread use so far because CSDA-based models could explain the interaction of electron beams with bulk solids reasonably well (at least in terms of the overall trends) with a fraction of the computational complexity. However, our approach seems to be suitable for studying the interaction between electron beams with nanostructures. A set of known cross-sections were used to calculate the discrete energy losses and the method was validated by comparing the results with the available experimental data. Further experimental investigation is needed in order to gain a better understanding of the role of each scattering process toward SE emission.

ACKNOWLEDGMENTS

We thank the Natural Sciences and Engineering Research Council (NSERC) for financial support. M.K.A. also thanks the University of British Columbia for a graduate fellowship.

[1]N. de Jonge and J. M. Bonard, Philosophical Transactions of the Royal Society A **362**, 2239 (2004).
[2]W. S. Kim, W. Yi, S. G. Yu, J. Heo, T. Jeong, J. Lee, C. S. Lee, J. M. Kim, H. J. Jeong, Y. M. Shin, and Y. H. Lee, Appl. Phys. Lett. **81**, 1098 (2002).
[3]A. Nojeh, W.-K. Wong, E. Yieh, R. F. W. Pease, and H. Dai, J. Vac. Sci. Technol. B **22**, 3124 (2004).
[4]P. Yaghoobi and A. Nojeh, Mod. Phys. Lett. B **21**, 1807 (2007).
[5]Y. Saito, *Carbon Nanotube and Related Field Emitters* (Wiley-VCH, Weinheim, 2010).
[6]T. Brintlinger Y.-F. Chen T. Dürkop, E. Cobas, M. S. Fuhrer, J. D. Barry, and J. Melngailis, Appl. Phys. Lett. **81**, 2454 (2002).
[7]P. Finnie, K. Kaminska, Y. Homma, D. G. Austing, and J. Lefebvre, Nanotechnology **19**, 335202 (2008).
[8]Y. Homma, S. Suzuki, Y. Kobayashi, M. Nagase, and D. Takagi, Appl. Phys. Lett. **84**, 1750 (2004).
[9]D. C. Joy, *Monte Carlo Modeling for Electron Microscopy and Microanalysis* (Oxford University Press, New York, 1995).
[10]M. Dapor, *Electron-Beam Interactions with Solids: Application of the Monte Carlo Method to Electron Scattering Problems* (Springer, New York, 2003).
[11]D. Drouin, A. R. Couture, D. Joly, X. Tastet, V. Aimez, and R. Gauvin, Scanning **29**, 92 (2007).
[12]R. Browning, T. Z. Li, B. Chui, J. Ye, R. F. W. Pease, Z. Czyzewski, and D. C. Joy, J. Appl. Phys. **76**, 2016 (1994).
[13]R. Shimizu, Y. Kataoka, T. Matsukawa, T. Ikuta, K. Murata, and H. Hashimoto, J. Phys. D **8**, 820 (1975).
[14]R. Browning, T. Z. Li, B. Chui, J. Ye, R. F. W. Pease, Z. Czyzewski, and D. C. Joy, Scanning **17**, 250 (1995).
[15]N. W. M. Ritchie, Surf. Interface Anal. **37**, 1006 (2005).
[16]R. Gauvin, E. Lifshin, H. Demers, P. Horny, and H. Campbell, Microsc. Microanal. **12**, 49 (2006).
[17]C. G. H. Walker, M. M. El-Gomati, A. M. D. Assa'd, and M. Zadrazil, Scanning **30**, 365 (2008).
[18]K. Murata, M. Yasuda, and H. Kawata, Scanning **17**, 228 (1995).
[19]R. Shimizu, Y. Kataoka, T. Ikuta, T. Koshikawa, and H. Hashimoto, J. Phys. D **9**, 101 (1976).
[20]M. K. Alam, P. Yaghoobi, M. Chang, and A. Nojeh, Appl. Phys. Lett. **97**, 261902 (2010).
[21]X. Liang, Z. Fu, and S. Y. Chou, Nano Lett. **7**, 3840 (2007).
[22]M. K. Alam, P. Yaghoobi, and A. Nojeh, J. Vac. Sci. Technol. B **28**, C6J13 (2010).
[23]M. K. Alam, P. Yaghoobi, and A. Nojeh, Scanning **31**, 221 (2009).
[24]M. M. Brzhezinskaya and E. M. Baitinger, *Trends in Nanotube Research* (Nova Science Publishers, New York, 2006).
[25]G. Chiarello, E. Maccallini, R. G. Agostino, V. Formoso, A. Cupolillo, D. Pacile, E. Colavita, L. Papagno, L. Petaccia, R. Larciprete, S. Lizzit, and A. Goldoni, Carbon **41**, 985 (2003).
[26]B. J. LeRoy, S. G. Lemay, J. Kong, and C. Dekker, Nature (London) **432**, 371 (2004).
[27]L. Reimer, *Scanning Electron Microscopy: Physics of Image Formation and Microanalysis* (Springer, Berlin, 1998).
[28]L. N. Pandey and M. L. Rustgi, J. Appl. Phys. **66**, 6059 (1989).
[29]F. Arezzo, N. Zacchetti, and W. Zhu, J. Appl. Phys. **75**, 5375 (1994).
[30]J. Quinn, Phys. Rev. **126**, 1453 (1962).
[31]N. V. Smith and W. E. Spicer, Phys. Rev. **188**, 593 (1969).
[32]D. C. Joy and S. Luo, Scanning **11**, 176 (1989).
[33]M. H. Gass, U. Bangert, A. L. Bleloch, P. Wang, R. R. Nair, and A. K. Geim, Nat. Nanotechnol. **3**, 676 (2008).
[34]R. Ferrell, Phys. Rev. **101**, 554 (1956).
[35]D. Drouin, P. Hovington, and R. Gauvin, Scanning **19**, 20 (1997).
[36]Z. Czyzewski, D. O'Neill MacCallum, A. Romig, and D. C. Joy, J. Appl. Phys. **68**, 3066 (1990).
[37]X. Wei, D. Golberg, Q. Chen, Y. Bando, and L. Peng, Nano Lett. **11**, 734 (2011).
[38]J.-Y. Park, S. Rosenblatt, Y. Yaish, V. Sazonova, H. Üstünel, S. Braig, T. A. Arias, P. W. Brouwer, and P. L. McEuen, Nano Lett. **4**, 517 (2004).
[39]A. Rivacoba and F. J. García de Abajo, Phys. Rev. B **67**, 085414 (2003).
[40]D. C. Joy, Scanning **17**, 270 (1995).
[41]D. Emfietzoglou, I. Kyriakou, R. Garcia-Molina, I. Abril, and K. Kostarelos, J. Appl. Phys. **108**, 054312 (2010).
[42]O. Stéphan, D. Taverna, M. Kociak, K. Suenaga, L. Henrard, and C. Colliex, Phys. Rev. B **66**, 155422 (2002).
[43]M. K. Alam, S. P. Eslami, and A. Nojeh, Physica E **42**, 124 (2009).